







Research Article

Effect of Friction Stir Welding on the Mechanical and Microstructural Behaviour of AA7075 Aluminium Alloy

C. R. Mahesha ¹, **R. Suprabha** ¹, **Nellore Manoj Kumar** ², **Koushik Kosanam** ³,
Harishchander Anandaram ⁴, **S. C. V. Ramana Murty Naidu** ⁵,
M. Kalyan Chakravarthi ⁶, and **Venkatesan Govindarajan** ⁷

¹Department of Industrial Engineering and Management, Dr. Ambedkar Institute of Technology, Bangalore 560056, India

²Department of Mathematics, Saveetha School of Engineering, Saveetha Institute of Medical and Technical Sciences (SIMATS), Thandalam, Chennai, Tamilnadu 602105, India

³Department of Manufacturing Systems Engineering & Management, California State University, 18111 Nordhoff St, Northridge, CA 91330, USA

⁴Centre for Excellence in Computational Engineering and Networking, Amrita Vishwa Vidyapeetham, Coimbatore, Tamil Nadu 641112, India

⁵Department of Mechanical Engineering, Sri Venkateswara College of Engineering and Technology, Srikakulam, Andhra Pradesh 532001, India

⁶School of Electronics Engineering, VIT-AP University, Amaravathi 522237, India

⁷Department of Mechanical Engineering, Haramaya Institute of Technology, Haramaya University, Dawa, Ethiopia

Correspondence should be addressed to Venkatesan Govindarajan; venkatesanggg2011@gmail.com

Received 21 June 2022; Accepted 25 August 2022; Published 10 September 2022

Academic Editor: Pudhupalayam Muthukutti Gopal

Copyright © 2022 C. R. Mahesha et al. This is an open access article distributed under the Creative Commons Attribution License, which permits unrestricted use, distribution, and reproduction in any medium, provided the original work is properly cited.

In this research work, an attempt was made to weld AA7075 alloy using the friction stir welding (FSW) technique. The experimental runs were designed using the Taguchi L18 orthogonal array and welds were obtained by varying tilt angle, tool rotation speed, tool feed rate, and axial load, whereas weld quality was accessed in terms of tensile strength and microhardness. The microstructure was examined using an optical microscope. The studies revealed that the tool angle was the most influential factor followed by the tool feed rate as both the parameters impacted the intensity of heat developed. It was observed that the tool tilt decreased the microhardness of the welds. The UTS values and macrostructure imply that the weld should be subjected to higher tool torque conditions. The material flow was not periodic nor coordinated, as seen by the tool-tilted weld's macrostructure. With a tool tilt, the weld pressure is lowered, and the lower pressure could not be enough to prevent volumetric defects. The reduced pressure at quicker welding rates may have had an effect on the development of flaws.

1. Introduction

AA7075, an aerospace aluminium alloy, has found its application in the manufacturing of aircraft structural wings and fins [1]. Zinc, a major alloying element of seven series aluminium alloy, possess a melting point of 420°C and boiling point of 907°C [2]. When joined utilizing the fusion welding technique, these zinc particles get evaporated, which alters the elemental composition of the aluminium alloy [3]. To overcome these issues, it was preferred to machine the

aerospace aluminium alloy with solid state welding techniques [4]. Friction stir welding (FSW), cold metal transfer (CMT), ultra-sonic welding (USW), and hot pressure welding (HPW) are the distinct solid state welding process [5]. In joining innovation, FSW has drawn in an extraordinary consideration as a strong-state welding procedure used to join comparable and different ferrous and nonferrous metals with practically no deformities [6]. FSW can stay away from the vast majority of the issues related to unique nonferrous materials joined by fusion welding processes [7].

Tool geometry, rotation speed, feed rate, and dwell time are the distinct process parameters deciding the quality of the welded joints [8]. While the tool is being translated, the material being stirred is being moved from the front to the rear of the tool probe while it is being rotated [9]. The quality of the weld is also impacted by the tool's axial pressure [10]. It means that extremely high pressures cause excessive heating and joint thinning, whereas extremely low pressures result in inadequate heating and voids [11]. Another crucial factor, particularly for creating welds with "smooth" tool shoulders, is the tool's tilt angle, as measured in relation to the work piece surface [12]. The Al (6061) and (1018 steel) sheets were joined by Chen et al. using Friction Stir Welding to create a 6 mm thick layer of each alloy. They employed a steel welding instrument to complete the butt joint. The sizes for the shoulder and pin were chosen to be 24 mm and 5.5 mm, respectively. On the side facing forward, they utilized aluminium sheet, and on the side facing back, steel. An optical microscope was used to find the metallographic analysis. They claimed that intermetallic compounds are present in the joint region, especially in the nugget field. At a distance of 100 mm and a rotational speed of 917 rpm, the tool snapped [13].

Muthu and Jayabalan focused on the microstructure and temperature dispersion of the weld produced by the friction mix welding technique between Al (6061-T6) and 99.9% copper [14]. They observed that there existed metallic mixes such as CuAl₂, CuAl, and, furthermore, Cu₉Al₄ buried in the joint field. According to them, there is a range of temperature conveyance and a high level of strong dissolvability in the bottom portion of the chunk location. Conductivity is a problem when welding copper in contact with other metals. They discovered that copper, due to its strong conductivity, diffuses the intensity created by the sponsorship blacksmith's iron, resulting in an inadequate welding temperature in the joint field. They discovered that the aluminium side's most severe temperature is 580 °C, which is greater than the softening point of the Al-Cu amalgam. They used 95 mm/min travel speed and 914 rpm rotating speed as the welding boundaries in this investigation. The friction mix welding apparatus used for this project was composed of steel [15]. From the above literature review, it was clear that a lot of research has been conducted on the welding of the aluminium alloy utilizing the FSW technique, research related to the FSW of AA7075 alloy and analysing its microstructural behaviour was very scarcely available. Hence, in this research work, an attempt was made to FSW AA7075 alloy by varying the input variables tilt angle, speed, feed, and axial load. The impact of these axial loads on the mechanical and microstructural behaviour was exploited deeply.

2. Experimental Work

The base metal utilized in the analyses was AA 7075 aluminium alloy with the chemical composition as depicted in Table 1. The experimental results are shown in Table 2 [16]. The following parametric limits were considered for the FSW; tool rotational speed (N), feed rate (S), axial force (F),

TABLE 1: Chemical composition of the AA7075 alloy (Spectrum analysis).

Element	Si	Fe	Cu	Mn	Mg	Cr	Zn	Al
Composition	0.07	0.25	1.6	0.07	2.6	0.3	5.9	Remaining

and tilt angle. Other variables, viz shoulder and pin diameter, were kept consistent to concentrate the impact of tool angle on weld arrangement. As a thumb rule, the instrument pin width was proposed as equivalent to the thickness of the parent metal, and the shoulder measurement was three times that of the pin diameter. In accordance with shoulder distance and pin, they were fixed at 18 mm and 6 mm separately. The trial grid was designed as per the Taguchi L18 symmetrical cluster. FSW was done on an 11 kV/440 V (AC) direct FSW machine. The table showed the exploratory plan lattice, which is a symmetrical exhibit with two degrees of boundaries. Three samples were sheared crossover to the weld crease from each example in a processing machine. The samples were prepared in conformance with American Society for Testing and Materials (ASTM) standard E8M-04 for the tensile tests. The typical worth of the elasticity was considered for each example. For microstructure, specimens were sheared wise to the weld line and cleaned and carved with Keller's reagent. A Trinocular metallurgical magnifying lens (TMM) was utilized to inspect the microstructure of the weld. The difference in mechanical properties of the weld joints was analysed through hardness estimations across the crossover, the cross part of the weld. Estimations were taken by a Vicker's hardness analyser at 0.5 kgf load with a dwell time of 10 sec. Readings were taken 1.5 mm beneath the weld zone and at an interval of 1 mm.

3. Results and Discussion

To validate the absence of potential flaws such as blazes and surface passage as depicted in Figure 1(a) and the tensile specimen as portrayed in Figure 1(b), all welds underwent a visual inspection. Welded seams had smooth surfaces and were clearly free of defects. Due to weld fusions that were formed at higher temperatures, the weld surface was rough and contained tiny aluminium particles that gave it a rough, paper-like look. However, upon ocular inspection, low temperature welds seemed to have smooth surfaces.

The ultimate tensile strength (UTS) for the joints manufactured at different parametric levels is shown in Figure 2. The outcomes showed that elasticity experienced a critical plunge as the instrument was shifted by a point of +1.50. The most extreme elasticity was accounted for a tilt angle of 0° indeed, even at a higher device travel speed of 600 mm/min. This movement speed is one of the greatest qualities at any point announced for AA7075 amalgam at a thickness of 6 mm. The microhardness for two instances is shown in Figure 3 as a delegate model; one with a tool angle of 0, 700 mm/min, and the other with 1.50, 600 mm/min, and 700 rpm. Welds made with 1.50 slant points revealed lower values for hardness, and the microhardness appropriation amply demonstrated the influence of tool angle.

TABLE 2: Experimental runs and its results.

S.No	Tilt angle	Tool rotation (rpm)	Tool feed rate (mm/min)	Axial load	Tensile strength (MPa)	Microhardness (HV)
1	0	500	16	10	248	63
2	0	500	20	15	311	68
3	0	500	24	20	272	71
4	0	600	16	10	299	59
5	0	600	20	15	342	66
6	0	600	24	20	322	70
7	0	700	16	15	287	64
8	0	700	20	20	261	68
9	0	700	24	10	339	72
10	1.5	500	16	20	304	43
11	1.5	500	20	10	352	48
12	1.5	500	24	15	278	47
13	1.5	600	16	15	255	51
14	1.5	600	20	20	286	39
15	1.5	600	24	10	322	55
16	1.5	700	16	20	347	44
17	1.5	700	20	10	326	42
18	1.5	700	24	15	303	49



FIGURE 1: (a) Visual inspection of the FSW joint. (b) FSW tensile specimen.

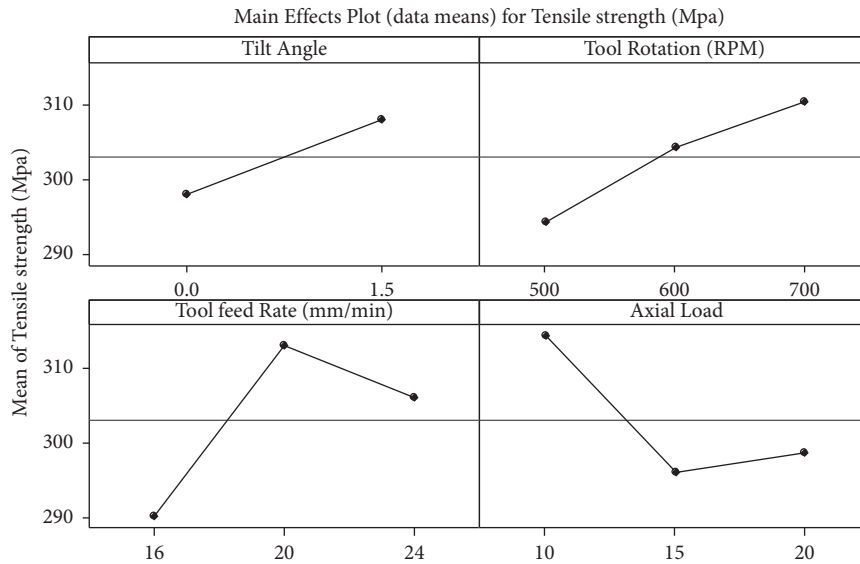


FIGURE 2: Main effect plot for tensile strength of FSW joints.

According to distinct research, the value of hardness is higher on the progressive side. In the case of a 0° tool angle, it is observed that the microhardness of the welds is approximately 70 Hv, resulting in a condition of up to 63 percent comparable with the base material hardness, while the microstructure hardness value is reduced to 45 in the case of a 1.50 tool angle.

The modification of the welds' mechanical characteristics with different process variables was demonstrated by variance in UTS and MH. For welds delivered with a tool tilt at a point of 1.5°, a significant decline in rigidity was observed. A similar trend was observed for the FSW of polyethylene. However, the general consensus was that increased strength for FSW joints of aluminium composites is favoured by a

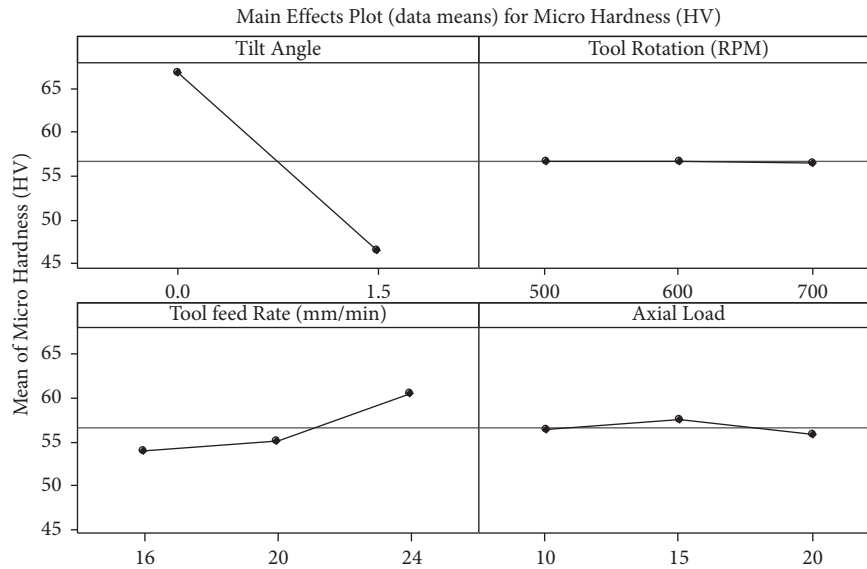


FIGURE 3: Main effect plot for microhardness of FSW joints.

tool tilt. The elasticity of the welds is improved by an instrument slant, according to a miniature underlying depiction of rubbing mix welded steel joints [17]. The device slant is the most effective boundary for the rigidity of the weld joints. Research promoting the notion that a tilt angle encourages blending and periodic replenishment of material in the weld joint, and the suppression of discharged material in the weld line by the tool shoulder has been taken into account [18]. In any event, a tool offset at higher rates may not be successful in achieving constraint and blending of extruded material, as seen by the drop in the weld strength included in this investigation. The microstructure has been used to assess the variation in UTS and microhardness.

The microstructure demonstrated precipitation solidification of the base metal following solution treatment. As shown in Figure 4(a), the main aluminium strong arrangement included fine, uniform Mg₂Si eutectic particles that had accelerated. The material was rolled, as seen by the direction of the grain. The grain direction might be observed along the path of the equal lines. The micrograph also shows a small amount of the insoluble intermetallic complex Al₆(Fe Mn) in the base metal structure. In both the cases, fracture of the eutectic particles happened at the shoulder zone (SZ) because of the strain of the turning shoulder. The insoluble buried metallic compounds have shaped a bunch at the shoulder zone, as found in Figures 4(b) and 4(c).

In the optical microscope, the nugget zones (NZ) of the two instances are identical. The NZ exhibit split eutectic Mg₂Si particles that have undergone distinctive recrystallization, as expected from Figures 5(a) and 5(b). The lack of grain direction, which was present in the parent metal, is thought to be the reason for the evidence of recrystallization. The eutectic particles would have disintegrated and quickly reprecipitated due to the mixing pressure and heated impact. For various welds produced under distinct input variables, the microstructure did not demonstrate a striking distinction. Therefore, it seems sensible to assume that heat input

was crucial for the welders, and errors in certain welds may be attributed to a shortage in the material stream. This notion is supported by the welds' macrostructure at various interfaces. The FSW joining system may be understood in terms of material forging and extrusion. As the pin spins, heat generated by friction softens the material, which is then released around the pin and produced by shoulder motion. For this activity to be viable, the rotational and crossover speeds must be combined properly. It is essential to add heat to the material in order to soften it so that the ejected material may be blended properly. It was determined that low intensity input was the main cause of kissing bond or poor passage.

A consistent and steady state FW was performed under fractional tacky and sliding interface contact conditions aside from the device plunge stage [19]. All things considered, at higher speeds, tacky contact conditions overwhelm the cycle. Thus, at higher velocities, tool force will be high. Different examinations have recommended that, besides in the instances of overheating, tool force has a direct relation to work piece hardness, yield strength, and ductility. As the welding speed increments, heat input diminishes, and power consumed builds, in view of the decreased time for material deformation and dispensation. In addition, at higher welding speeds, the material ahead of the pin gets an extension period to preheat the material in the encompassing, and this retards the material softening for the welding system, which requires higher axial force. In such a condition, the intensity input depends generally on the plastic deformity of the encompassing mass material. In FSW, the info power is changed over into plastic softening energy, which is to some degree put away in the microstructure and to some extent changed over into heat. The consequences of mathematical re-enactments uncover that the heat energy gotten from plastic twisting shifts from 2 to 20% [20]. These perceptions prove low heat contribution at higher welding speeds. The general pattern of low UTS in all welds was

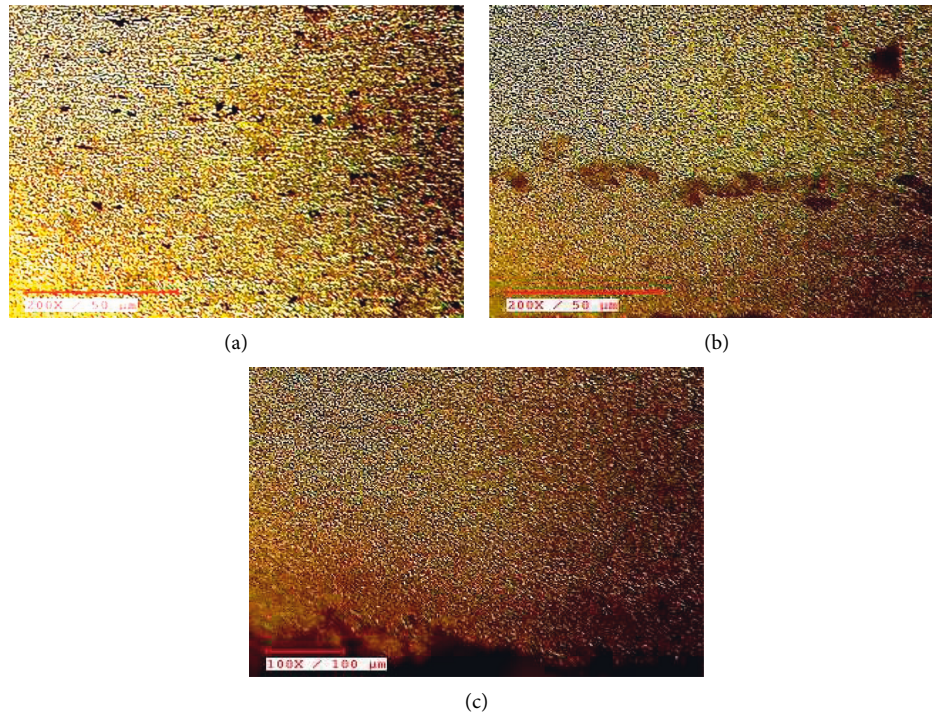


FIGURE 4: Microstructure of the (a) base metal, (b) shoulder zone with 0° tool angle, and (c) shoulder zone with 1.5° tool angle.

characteristic of low heat input for the scope of welding speed.

The majority of the heat in FSW was produced by shoulder activity, and the material stream was also impacted by the shoulder's crucial stress on plasticized material. The pin action regulates the material union and sporadic material filling of the joint. The substance is transported upward on the withdrawing side while being pushed downward on the pushing side [21]. The device strings pull the material below while moving the material in front of the pin upward [22]. The tool tilts in favour of the material's vertical growth in front of the pin. Other limits, such as pivotal power, rotational speed, and welding speed, have an impact on the union through the intermittent interchange of material. Although the shoulder driven stream and pin driven stream procedures are unaffected, the single stream volume and then the full mix zone are factors in welding speed [23]. The welding speed may thus have a greater influence on the material stream.

The device activity's material evolution in FSW is challenging. The split of the material handling zone into a revolution zone and a progress zone was suggested by Behera et al. [24]. The material stream is a combination of crossover, longitudinal, and exact, as for the device hub in the revolution zone, which is promptly located on the device pin surface. The progress zone was identified as the shear layer of material located between the rotational zone and the material framework. Heat input is a factor in the overall grinding mix volume.

In FSW, the weld formation proceeds while the material filling is delayed. By filling the material holes sporadically to provide a weld without deformities, a successful mix of

boundaries overcomes this time delay. Due to this period of time where the grooves are not compensated by the compelling material stream, passage swindles have developed. Weld zones can be divided into shoulder-affected zones (SAZ), pin impacted zones (PIZ), and weld base zones (WBZ) depending on the material stream. Trench deformation is thought to be caused by a time delay in material filling in the PAZ. The descending material stream in the SAZ is reduced and surrenders are therefore created if the material stream from the withdrawing side to the pushing side and/or the crucial power are insufficient. It was explained that the material stream in the SAZ is persistent because the material in contact with the shoulder pivots at the same speed as the equipment. The material streams in the PAZ spin with the hardware and also move in an upward and downward orientation. As a result, the material stream in the PAZ is variable. The WBZ, which is located between the equipment tip and the parent metal's base surface, typically has a low stream speed of material. During the instrument's direct development, the WBZ is filled with material. WBZ is always filled at the point where the equipment passes the weld line at any given time. The weld setup in the WBZ needed more time in this fashion [25, 26].

The weld's macrostructure reveals an extremely sizable amount of void at the pin's bottom portion. Such malformations have been caused by inadequate intensity input that led to a viral weld situation [27, 28]. This situation, and the development of the vacuum into a passage or worm opening defect, may have been energised by a higher welding rate. The material around the FSW pin creeps around it, and it also streams upward in a roughly spherical form in layers [29, 30]. Ineffective material mixing is seen in Figure 5. 8 at



FIGURE 5: Microstructure of the NZ (a) at 0° tool angle and (b) at 1.5° tool angle.

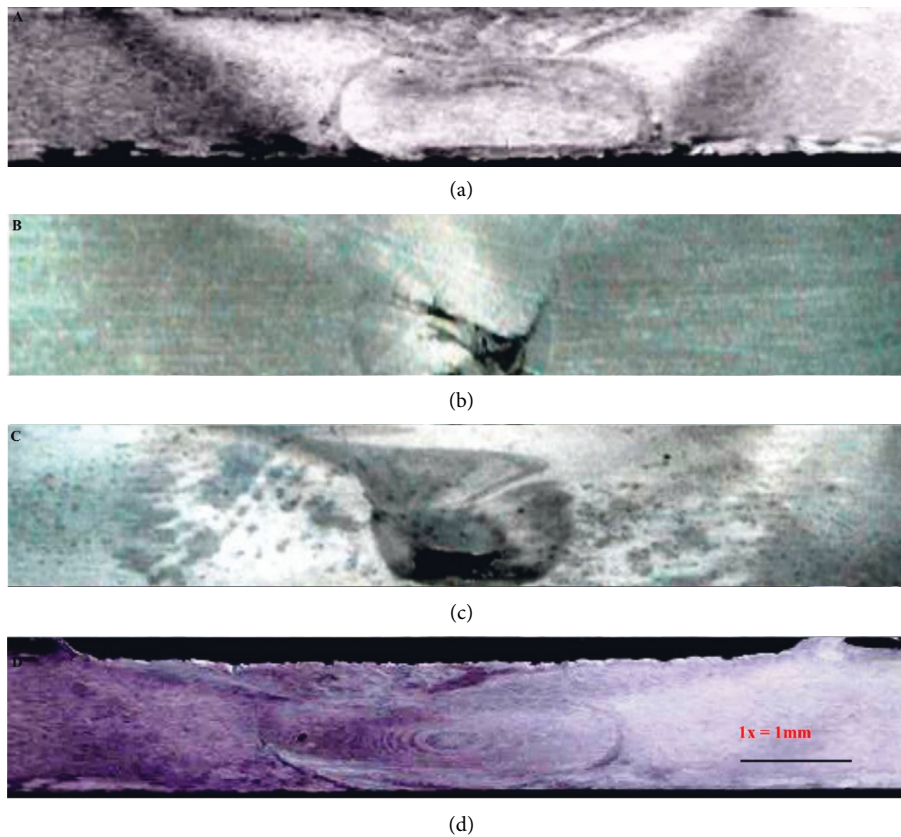


FIGURE 6: Macroscopic view of (a) weld at 0° tool angle, (b) weld at 1.5° tool angle, (c) weld with tunnel, and (d) distinct weld zones.

various contact levels. Possible causes include inadequate material flow around the pin and a lack of sufficient SAS, PAZ, and WBZ manufacturing activity by the shoulder. The mathematical components of the strung pin will probably not be an option for the device to tilt at greater rates in order to achieve the proper material stream. It may have resulted in the interior crumbling and regenerating.

In Figure 6(a), the macrostructure of the weld created at a 0° tilt angle is shown. The macrostructure demonstrates that the weld was freed from substantial flaws. The NZ was

typically better than other weld types. It was explained that the pivoting pin, which in FSW is referred to as the turning shear material, deforms the material immediately adjacent to the apparatus surface (TSM). When a threaded pin profile is offered, the forcefully deformed material from the apparatus pin string surface pulls the surrounding material by the pinning activity. This surrounding stream, TSM, and the shoulder-driven material sporadically fill the hole when the tool progression occurs to prevent the development of volumetric defects. The size of the NZ determines the

superior material stream and mechanical qualities since larger NZs display suitable shoulder-driven streams. The material stream in the macrostructure showed the formation of onion rings. When compared to other welds, the superior material transformation and combination of this one may be to blame for the improved mechanical characteristics.

Inadequate material stream caused deformities of insufficient filling, as seen in Figures 6(b) and 6(c), in the macrostructure of the welds generated at a 1.5° device tilt angle. To prevent the creation of deformities, shoulder-driven material has to be properly convergent with pin-driven material [31, 32]. This material flow strategy relies heavily on temperature and axial power. It is logical to assume that the slanted point of the instrument, at the higher crossing speed, adversely influences the material stream and consolidation of layered material during welding and causes deformity arrangement because the tilt angle affects the shoulder-driven material stream and hydrostatic tension. According to FSW of AA 7075, the material stream is supposedly sensitive to the shoulder [33, 34]. The vertical power following up on the weld line is altered as the instrument is adjusted. This might affect the amount of material sucked in by the shoulder and the intensity that is generated. This effect could be anticipated to become significant at a faster rate. This might provide an explanation for the age of flaws that appear when the device is moved, as seen in the macrograph in Figure 6(d).

4. Conclusion

Along with other process factors, the impact of tool tilt angle on the high-speed FSW of 7075 aluminium alloy was investigated. An ideal set of process parameters was then provided. The outcomes of the research showed that

- (1) The most important factor influencing weld strength is tool tilt angle, which has been demonstrated to have a negative impact on weld strength at faster tool travel speeds.
- (2) Although the welds made at faster rates appeared to be free of defects, it was found that they had relatively weak welds, especially when the tool is tilted.
- (3) The tool tilt was found to reduce the microhardness of the welds. Higher tool torque conditions for the weld are suggested by the UTS values and macrostructure. The macrostructure of the tool-tilted weld demonstrates that the material flow was neither periodic nor coordinated.
- (4) Weld pressure is decreased with a tool tilt, and the reduced pressure may be less than the limiting amount needed to prevent volumetric flaws. The creation of defects may have been impacted by the lower pressure at faster welding speeds.

Data Availability

The data used to support the findings of this study are included within the article.

Conflicts of Interest

The authors declare that there are no conflicts of interest.

References

- [1] S. Rajakumar, C. Muralidharan, and V. Balasubramanian, "Influence of friction stir welding process and tool parameters on strength properties of AA7075-T6 aluminium alloy joints," *Materials & Design*, vol. 32, no. 2, pp. 535–549, 2011.
- [2] A. Nishimoto, J. I. Inagaki, and K. Nakaoka, "Influence of alloying elements in hot dip galvanized high tensile strength sheet steels on the adhesion and iron-zinc alloying rate," *Tetsu-To-Hagane*, vol. 68, no. 9, pp. 1404–1410, 1982.
- [3] H. Nagaseki and K. I. Hayashi, "Experimental study of the behavior of copper and zinc in a boiling hydrothermal system," *Geology*, vol. 36, no. 1, pp. 27–30, 2008.
- [4] E. Akca and A. Gürsel, "Solid state welding and application in aeronautical industry," *Periodicals of Engineering and Natural Sciences*, vol. 4, no. 1, 2016.
- [5] A. Nassiri, T. Abke, and G. Daehn, "Investigation of melting phenomena in solid-state welding processes," *Scripta Materialia*, vol. 168, pp. 61–66, 2019.
- [6] R. Ranjith and B. Senthil Kumar, "Joining of dissimilar aluminium alloys AA2014 T651 and AA6063 T651 by friction stir welding process," *WSEAS Transactions on Applied and Theoretical Mechanics*, vol. 9, pp. 179–186, 2014.
- [7] D. Kumar Rajak, D. D. Pagar, P. L. Menezes, and A. Eyvazian, "Friction-based welding processes: friction welding and friction stir welding," *Journal of Adhesion Science and Technology*, vol. 34, no. 24, pp. 2613–2637, 2020.
- [8] D. Mishra, R. B. Roy, S. Dutta, S. K. Pal, and D. Chakravarty, "A review on sensor based monitoring and control of friction stir welding process and a roadmap to Industry 4.0," *Journal of Manufacturing Processes*, vol. 36, pp. 373–397, 2018.
- [9] M. Abbasi, A. Abdollahzadeh, B. Bagheri, A. Ostovari Moghaddam, F. Sharifi, and M. Dadaei, "Study on the effect of the welding environment on the dynamic recrystallization phenomenon and residual stresses during the friction stir welding process of aluminum alloy," *Proceedings of the Institution of Mechanical Engineers - Part L: Journal of Materials: Design and Applications*, vol. 235, no. 8, pp. 1809–1826, 2021.
- [10] F. Lambiase, H. A. Derazkola, and A. Simchi, "Friction stir welding and friction spot stir welding processes of polymers—state of the art," *Materials*, vol. 13, no. 10, p. 2291, 2020.
- [11] K. P. Mehta, R. Patel, H. Vyas, S. Memon, and P. Vilaça, "Repairing of exit-hole in dissimilar Al-Mg friction stir welding: process and microstructural pattern," *Manufacturing Letters*, vol. 23, pp. 67–70, 2020.
- [12] R. Ranjith, P. K. Giridharan, and K. B. Senthil, "Predicting the tensile strength of friction stir welded dissimilar aluminum alloy using ANN," *International Journal of Civil Engineering & Technology*, vol. 8, no. 9, pp. 345–353, 2017.
- [13] G. Chen, S. Zhang, Y. Zhu, C. Yang, and Q. Shi, "Thermo-mechanical analysis of friction stir welding: a review on recent advances," *Acta Metallurgica Sinica*, vol. 33, no. 1, pp. 3–12, 2020.
- [14] M. F. X. Muthu and V. Jayabalan, "Tool travel speed effects on the microstructure of friction stir welded aluminum-copper joints," *Journal of Materials Processing Technology*, vol. 217, pp. 105–113, 2015.
- [15] Y. Sun, W. Gong, J. Feng, G. Lu, R. Zhu, and Y. Li, "A review of the friction stir welding of dissimilar materials between

- aluminum alloys and copper,” *Metals*, vol. 12, no. 4, p. 675, 2022.
- [16] K. S. Arora, S. Pandey, M. Schaper, and R. Kumar, “Effect of process parameters on friction stir welding of aluminium alloys 2219-T87,” *The International Journal of Advanced Manufacturing Technology*, vol. 50, no. 9, pp. 941–952, 2010.
- [17] S. M. Senthil, R. Parameshwaran, S. Ragu Nathan, M. Bhuvanesh Kumar, and K. Deepandurai, “A multi-objective optimization of the friction stir welding process using RSM-based-desirability function approach for joining aluminum alloy 6063-T6 pipes,” *Structural and Multidisciplinary Optimization*, vol. 62, no. 3, pp. 1117–1133, 2020.
- [18] H. Jafari, H. Mansouri, and M. Honarpisheh, “Investigation of residual stress distribution of dissimilar Al-7075-T6 and Al-6061-T6 in the friction stir welding process strengthened with SiO₂ nanoparticles,” *Journal of Manufacturing Processes*, vol. 43, pp. 145–153, 2019.
- [19] W. Zhao and C. Wu, “Constitutive equation including acoustic stress work and plastic strain for modeling ultrasonic vibration assisted friction stir welding process,” *International Journal of Machine Tools and Manufacture*, vol. 145, Article ID 103434, 2019.
- [20] R. Saha and P. Biswas, “Current Status and Development of External Energy-Assisted Friction Stir Welding Processes: A Review,” *Welding in the World*, pp. 1–33, Springer, Berlin, Germany, 2022.
- [21] T. A. Shehabeldeen, M. A. Elaziz, A. H. Elsheikh et al., “A novel method for predicting tensile strength of friction stir welded AA6061 aluminium alloy joints based on hybrid random vector functional link and henry gas solubility optimization,” *IEEE Access*, vol. 8, pp. 79896–79907, 2020.
- [22] E. T. Akinlabi and R. M. Mahamood, *Solid-state Welding: Friction and Friction Stir Welding Processes*, Springer International Publishing, New York, NY, USA, 2020.
- [23] G. Chen, G. Wang, Q. Shi, Y. Zhao, Y. Hao, and S. Zhang, “Three-dimensional thermal-mechanical analysis of retractable pin tool friction stir welding process,” *Journal of Manufacturing Processes*, vol. 41, pp. 1–9, 2019.
- [24] R. K. Behera, B. P. Samal, S. C. Panigrahi, and K. K. Muduli, “Microstructural and mechanical analysis of sintered powdered aluminium composites,” *Advances in Materials Science and Engineering*, vol. 2020, pp. 1–7, Article ID 1893475, 2020.
- [25] M. Shunmugasundaram, A. Praveen Kumar, L. Ponraj Sankar, and S. Sivasankar, “Optimization of process parameters of friction stir welded dissimilar AA6063 and AA5052 aluminium alloys by Taguchi technique,” *Materials Today Proceedings*, vol. 27, pp. 871–876, 2020.
- [26] R. K. Behera, B. P. Samal, S. C. Panigrahi et al., “Erosion wear characteristics of novel ammc produced using powder metallurgy,” *Archives of Metallurgy and Materials*, vol. 67, no. 3, 2022.
- [27] A. Janeczek, J. Tomków, and D. Fydrych, “The influence of tool shape and process parameters on the mechanical properties of AW-3004 aluminium alloy friction stir welded joints,” *Materials*, vol. 14, no. 12, p. 3244, 2021.
- [28] R. K. Behera, B. P. Samal, S. C. Panigrahi et al., “Experimental analysis on machinability aspects of sintered aluminium metal matrix (Al+ Si+ Mg+ Cu+ SiC) composite-a novel product produced by powder metallurgy method,” *International Journal of Materials Engineering Innovation*, vol. 13, no. 1, pp. 1–22, 2022.
- [29] K. P. Mehta, P. Carlone, A. Astarita, F. Scherillo, F. Rubino, and P. Vora, “Conventional and cooling assisted friction stir welding of AA6061 and AZ31B alloys,” *Materials Science and Engineering*, vol. 759, pp. 252–261, 2019.
- [30] B. P. Samal, R. K. Behera, A. Behera et al., “Fuzzy logic application on dry sliding wear behavior of matrix aluminium composite produced by powder metallurgy method. Composites: mechanics, computations, applications,” *Composites: Mechanics, Computations, Applications, An International Journal*, vol. 13, no. 1, pp. 49–62, 2022.
- [31] S. Jayaprakash, S. Siva Chandran, T. Sathish et al., “Effect of tool profile influence in dissimilar friction stir welding of aluminium alloys (AA5083 and AA7068),” *Advances in Materials Science and Engineering*, vol. 2021, pp. 1–7, Article ID 7387296, 2021.
- [32] R. K. Behera, B. P. Samal, S. C. Panigrahi, K. Muduli, A. Mohamed, and A. Samal, “Evaluation of magnesium recovery in Al-Mg alloys produced by modified stir casting method using genetic algorithm optimisation technique,” *International Journal of Materials Engineering Innovation*, vol. 12, no. 2, pp. 134–148, 2021.
- [33] K. Fuse and V. Badheka, “Bobbin tool friction stir welding: a review,” *Science and Technology of Welding & Joining*, vol. 24, no. 4, pp. 277–304, 2019.
- [34] G. H. S. F. L. Carvalho, I. Galvão, R. Mendes, R. M. Leal, and A. Loureiro, “Friction stir welding and explosive welding of aluminum/copper: process analysis,” *Materials and Manufacturing Processes*, vol. 34, no. 11, pp. 1243–1250, 2019.